Inline amplification of mid-infrared intrapulse difference frequency generation

Q. Bournet, M. Jonusas, A. Zheng, F. Guichard, M. Natile, Y. Zaouter, M. Joffre, A. Bonvalet, F. Druon, Marc Hanna, et al.

Inline amplification of mid-infrared intrapulse difference frequency generation

Q. Bournet, M. Jonusas, A. Zheng, F. Guichard, M. Natile, Y. Zaouter, M. Joffre, A. Bonvalet, F. Druon, Marc Hanna, et al.

Inline amplification of mid-infrared intrapulse difference frequency generation

Q. Bournet[1,2,*], M. Jonusas[3], A. Zheng[1], F. Guichard[2], M. Natile[2], Y. Zaouter[2], M. Joffre[3], A. Bonvalet[3], F. Druon[1], M. Hanna[1], and P. Georges[1]

[1] Université Paris-Saclay, Institut d'Optique Graduate School, CNRS, Laboratoire Charles Fabry, 91127 Palaiseau, France
[2] Amplitude, 11 Avenue de Canteranne, Cité de la Photonique, 33600 Pessac, France
[3] Laboratoire d'Optique et Biosciences, Ecole Polytechnique, CNRS, INSERM, Institut Polytechnique de Paris, 91128 Palaiseau, France
[*] Corresponding author: quentin.bournet@institutoptique.fr

Compiled August 22, 2022

We demonstrate an ultrafast mid-infrared (MIR) source architecture that implements both intrapulse difference frequency generation (iDFG) and further optical parametric amplification (OPA), in an all-inline configuration. The source is driven by a nonlinearly compressed high-energy Yb-doped-fiber amplifier delivering 7.4 fs pulses at a central wavelength of 1030 nm, at a repetition rate of 250 kHz. It delivers 1 μJ, 73 fs pulses at a central wavelength of 8 μm, tunable over more than one octave. By enrolling all the pump photons in the iDFG process and recycling the long wavelength pump photons amplified in the iDFG in the subsequent OPA, we obtain an unprecedented overall optical efficiency of 2%. These performances, combining high energy and repetition rate in a very simple all-inline setup, make this technique ideally suited for a growing number of applications, such as high harmonic generation in solids or two-dimensional infrared (2DIR) spectroscopy experiments.

High repetition rate ultrafast sources in the mid-infrared (MIR) are currently being actively developed by a large research community because they are the workhorse for a growing number of applications, such as high-field physics in bulk and nanostructured solids [1, 2], field-resolved spectroscopy [3] or 2DIR spectroscopy [4–6]. In particular, 2DIR spectroscopy is ideally suited to assess protein conformational changes, opening a very large investigation field in the dynamics of biologically relevant molecules. These applications require the acquisition of a large number of 2DIR spectra with ultrashort pulses at high energy in the MIR. Recent research work on MIR sources has focused on combining high repetition rate diode-pumped laser sources with supercontinuum-seeded optical parametric amplification (OPA) systems of various degrees of complexity, sometimes with the addition of a difference frequency generation (DFG) stage. As demonstrated recently [7–9], a repetition rate around 100 kHz combines fast data averaging with the ability to acquire individual spectra for each laser shot for equilibrium 2DIR spectroscopy. These sources however suffer from relatively low conversion efficiencies (ratio between MIR energy and the total pump energy) (0.2% - 2.6% at 7-8 μm) [10–16].

Another generation method is to perform intrapulse DFG (iDFG) using a short enough pump pulse [17, 18]. Indeed, if the spectrum of the incident pump pulse covers a range that exceeds the desired optical frequency in the MIR, it is possible to realize a frequency difference between the extremal wavelengths of the pump spectrum, thus directly generating an ultrashort pulse in the MIR. Advantages of this approach include a very simple implementation, with inbuilt spatial/temporal superposition, and the generation of shorter MIR pulses than aforementioned systems. However, conversion efficiencies are generally even lower than OPA-based techniques (<0.5%, typically 0.1% at 6-10 μm) [3, 19–22]. This is due to the lower useful number of interacting pump photons because the spectral density of the ultrashort NIR pulse is distributed over a larger bandwidth and two linear polarization states. A few examples of iDFG/OPA systems pumped at 1 μm wavelength, thus benefiting from the mature ytterbium laser technology, have been recently demonstrated. In [23], MIR central wavelengths between 1.8 and 4.2 μm are generated with a Ti:Sa pump laser, using a coincident phase matching angle of DFG and OPA in a BiB_3O_6 (BIBO) crystal at a repetition rate of 1 kHz. Parametric amplification of iDFG from a Yb-based laser has also been demonstrated using an external non-broadened pump in a subsequent dual-OPA stage [24], at MIR wavelengths from 2.8 to 3.8 μm) and 6 kHz repetition rate.

In this work, we demonstrate that it is possible to recycle the pump radiation at the output of an iDFG stage to transfer part of its energy to the MIR pulse in a subsequent inline OPA stage. This idea bears similarities with cascaded THz generation [25], and extension to the MIR range was proposed theoretically [26]. Pumped by a few-cycle ytterbium laser system, the described ultrafast MIR source combines a chirp-management crystal, a bichromatic waveplate (BWP) [27, 28], a type II $LiGaS_2$ (LGS) crystal-based iDFG stage, a delay-management birefringent crystal, and a type I LGS crystal-based OPA stage. This implementation results in several key features: (i) all pump photons are polarized adequately to be enrolled in the iDFG process (ii) the long wavelength pump photons that have been amplified in the iDFG stage are available for recycling and used to pump

the OPA stage after a resynchronization stage (iii) the architecture is all inline, without alignment involved for both spatial and temporal overlaps. This architecture potentially overcomes the conversion efficiency limitations of iDFG-based MIR sources, allowing the generation of carrier-envelope phase stable 1 μJ 73 fs pulses at 250 kHz and a central wavelength of 8 μm, with a conversion efficiency of 2%. This unique set of parameters makes it very appealing for applications that benefit both from a high repetition rate and sufficient energy to drive highly nonlinear processes.

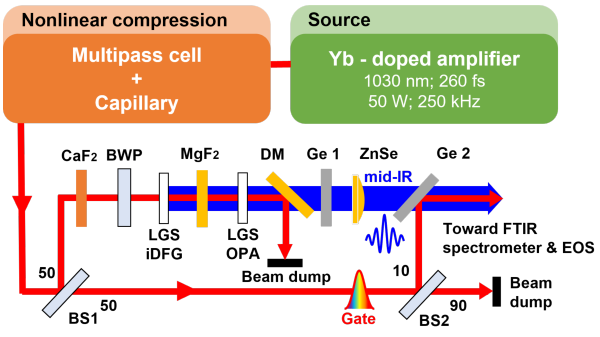

Fig. 1. Schematic of the experimental setup. The pump beam is sent on the 50/50 beamsplitter (BS1). The reflected driving pulses go through CaF_2 windows to adjust the chirp and the bichromatic waveplate (BWP). Then, they drive the generation in the XY LGS crystal and the amplification in the XZ LGS crystal. The MIR radiation is filtered by a dichroic mirror (DM). A germanium plate (Ge 1) is inserted to adjust the GDD of the MIR and a ZnSe lens is used to collimate it. A MgF_2 crystal is inserted to adjust the signal-MIR delay. The transmitted pulses (gate) are sent to a second beamsplitter (BS2) and to a second germanium plate (Ge 2) to recombine the gate and the MIR for the EOS measurement.

As shown in Fig. 1, the first part of the experimental setup is similar to the one presented in [28]. The initial pulses are produced by a high-energy Yb-doped-fiber amplifier delivering 200 μJ 250 fs pulses at a central wavelength of 1030 nm and at a repetition rate of 250 kHz. This source is followed by a 61% efficient dual-stage nonlinear compression scheme [29]. The spectrum, spectral phase, and temporal profile of the compressed pulses, measured using a d-scan system [30], are shown in Fig. 2. The pulse duration is 7.4 fs (see Fig. 2(b)), near the Fourier transform limited (FTL) pulse duration (7 fs), and the average power of this few-cycle beam is 30.5 W. We use half of this power to drive the MIR source using a broadband 50/50 beam splitter.

The MIR generation part starts with calcium fluoride (CaF_2) plates that are inserted to optimize the chirp of the input pulse prior to the iDFG stage. To enhance the efficiency of the iDFG process, we add a bichromatic waveplate (BWP) oriented at an angle of 45° between its axes and the input beam polarization to rotate the polarization state of the wavelengths below 1030 nm by 90° (later denoted as pump), while maintaining unrotated the polarization state of the wavelengths above 1030 nm (later denoted as signal) [28]. Note that we will keep using this denomination of "signal" for this beam even for the OPA stage where it really acts as a pump, and a second signal at a wavelength of around 1300 nm is generated. Then, an AR 900–1100 nm (R<1%) and 4–8 μm (R<4%) coated 1 mm-thick LGS crystal from Ascut UG & Co. KG. is used for iDFG. This crystal is phase

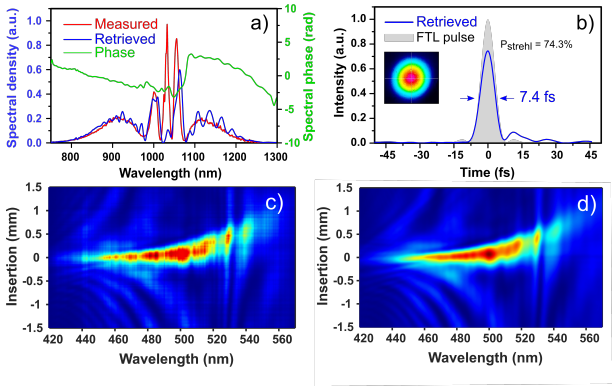

Fig. 2. (a) Independently measured (red) and d-scan retrieved (blue) spectra, and retrieved spectral phase (green) of the compressed driving pulses with 8 mm of CaF_2. (b) Corresponding temporal profile and measured far-field spatial profile in inset. (c) Measured and (d) retrieved d-scan traces.

matched in the XY plane at angles $\theta_{XY} = 90°$ and $\phi_{XY} = 44.1°$. It corresponds to phase matching for a pump beam at 900 nm polarized along the XY plane (later denoted e for extraordinary) and signal beam at 1100 nm along the Z-direction (later denoted o for ordinary). The idler beam in the mid-infrared is polarized along the e-direction, orthogonal to the signal beam. This will further allow convenient resynchronization using a birefringent material. The total average power incident on the LGS crystal is 13.2 W (53 μJ) with a $1/e^2$ diameter of 3.6 mm, corresponding to an estimated peak intensity of 140 GW/cm^2. After a dichroic mirror and a germanium plate to filter the MIR, we measure MIR average powers from 5 mW (at 4 μm) to 18 mW (at 8.6 μm) depending on the generated MIR wavelength and the thickness of the CaF_2 plates inserted (4 mm and 7 mm at 4 μm and 8.6 μm, respectively). See Table S1 in Supplementary Information section I for more details.

At the output of the iDFG crystal, while the pump is depleted, the signal pulse is amplified by the nonlinear process, and trails the MIR pulse by a delay that depends on the specific MIR wavelength. As mentioned earlier, this delay can be easily compensated using a birefringent plate (later denoted as time delay crystal), thereby allowing subsequent inline amplification of the MIR in a second LGS crystal. Another AR 900–1100 nm (R<1%) and 4–8 μm (R<4%) coated LGS crystal (later denoted as OPA crystal) phase matched in the XZ plane at angles θ_{XZ} of 49.8° and ϕ_{XZ} of 0° is used for this purpose. This corresponds to phase matching for the signal at 1100 nm polarized along the XZ plane and the idler MIR beam along the Y-direction (a "second" signal beam is generated in this process around 1300 nm, see Fig.S1 in Supplementary Information section I). A concave enhanced silver mirror with a radius of curvature RoC= 600 mm is used between the iDFG and OPA stages to loosely focus the beams in the OPA crystal. The beam sizes are 720 and 830 μm for the signal and MIR respectively. The incident average power is 11.8 W for the pump and signal, and 17 mW for the MIR. Due to the group velocity dispersion (GVD) of 300 fs^2 in the iDFG crystal, the calculated signal pulse duration after the generation stage is $\sim$ 70 fs corresponding to a peak intensity I $\sim$300 GW/cm^2. As time delay crystal, we choose uncoated magnesium fluoride (MgF_2) for the 4 to 6.5 μm MIR tunability range and a coated Y-cut LGS crystal for the 7.5 to 8.5 μm, where the transmission ranges are > 90% and > 80% respectively for these

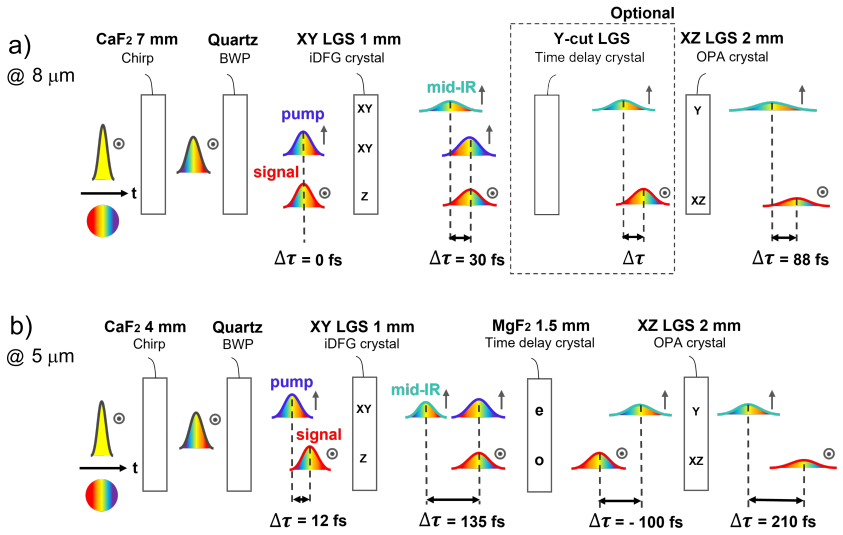

Fig. 3. (a) Time delay between the pump (blue), the signal (red) and the mid-infrared (cyan) pulses after each stage. The pulses are represented as a function of time. The central wavelengths considered are 950, 1050, and 8000 nm for the pump, signal and MIR idler respectively. (b) Same representation for a MIR central wavelength of 4700 nm. Pulse chirp is highlighted by the color code under the pulse envelope. The polarization of each pulse is indicated by arrows.

two materials. Fig. 3 shows the calculated time delay values through the inline architecture, for two different values of the MIR central wavelength.

For long wavelengths (around 8 μm) (Fig. 3(a)), a negligible signal-to-idler group velocity mismatch (GVM) and a high group delay dispersion (GDD) of -2850 fs²/mm on the MIR are introduced through the iDFG crystal, facilitating pulse temporal overlapping. Because the GVM remains small in the OPA crystal, no time delay crystal is needed. This was verified at a generated wavelength of 8 μm by measuring the MIR gain at the output of the OPA crystal while changing the delay obtained using various thicknesses of the Y-cut LGS crystal. The maximum amplification occurs when no time delay crystal is inserted, with a gain of 8.9.

For shorter MIR wavelengths (around 5 μm) (Fig. 3(b)), the MIR pulse is significantly faster than the signal one and leads by 135 fs at the output of the iDFG crystal. Moreover, the GDD induced by the first stage is smaller by one order of magnitude with regards to the previous case, further constraining the overlapping of the pulses at the input of the amplification stage. In addition, the GVM in the OPA crystal is $\sim$ 110 fs/mm, further distancing the MIR pulse from the signal one. As predicted from numerical simulations (see Fig. S2 in Supplementary Information section II) a 1.5 mm-thick MgF_2 plate is used (GVM = -160 fs/mm) to delay the MIR pulse by approximately 235 fs and pre-compensate the time delay at the input of the OPA crystal.

We now report on the spectral properties of the generated and amplified mid-infrared beams. Fig. 4(a) shows the spectrum tunability at the iDFG and OPA stages, for a 1 mm-thick iDFG crystal, a MgF_2 plate with a thickness that maximizes the gain, and a 3 mm-thick OPA crystal, obtained by adjusting ϕ_{XY} and θ_{XZ}. The MIR spectrum is tunable over a bandwidth extending from 4 to 8.5 μm, covering a range of more than one octave in the MIR. We measured energies from 35 nJ to 640 nJ leading to gains of 1.7 and 8.9 from one end of the tuning range to the other. The higher gains are due to very small GVM in the OPA crystal between the longest MIR wavelengths and the signal pulses.

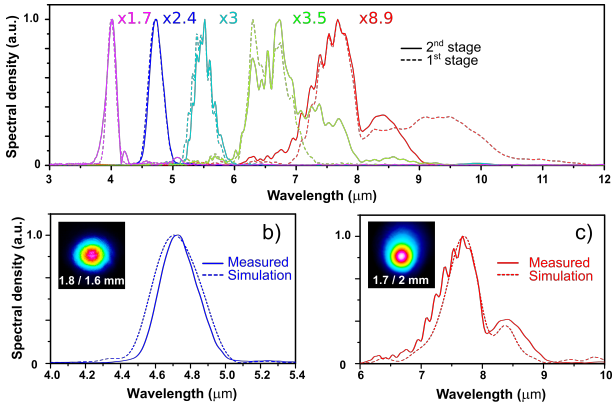

Fig. 4. (a) Measured tunability of the mid-infrared spectrum for the iDFG (dashed) and OPA (solid) stages, with corresponding OPA gains. (b) Measured (blue) and simulated (blue dashed) spectra of the amplified mid-infrared centered at 4.7 μm. (c) Measured (red) and simulated (red dashed) spectra of the amplified mid-infrared centered at 8 μm. All spectra are taken with the 1 mm-thick iDFG crystal and the 3 mm-thick OPA crystal.

This effect is demonstrated by several measurements using OPA crystals of different thicknesses: an energy of 1080 nJ (gain = 15) is reached at 8 μm for an 4 mm-thick crystal, corresponding to an overall optical efficiency of 2% (see Fig. S1 and Table S2 in Supplementary Information section I). The amplified spectra are narrowed, depending on the central wavelength, due to the spectral acceptance of the OPA LGS. Fig. 4(b) and (c) shows the measured spectra at the two representing wavelengths of the tunability range, both in good agreement with simulations. The output spatial profiles at 4.7 μm and 8 μm, shown in the insets of Fig. 4(b) and (c), are gaussian with ellipticities of 88% and 87%, respectively. One can notice that it is important to monitor the amplified spectrum (and not only the average power) dur-

ing the tunability process to avoid parasitic generations in the OPA crystal at other mid-IR wavelengths (see Supplementary Information section III).

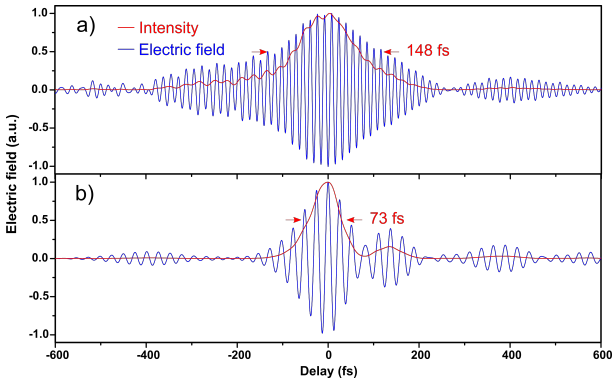

Fig. 5. (a) EOS trace (blue) and temporal intensity (red) of the mid-infrared pulse corresponding to a spectrum centered at 4.7 μm in Fig. 4(b), with an OPA crystal thickness of 3 mm. (b) Same measurement for a spectrum centered at 8 μm with an OPA crystal thickness of 4 mm. A large phase-matching bandwidth leads to shorter pulse durations at 8 μm.

Finally, an electro-optic sampling (EOS) setup is used to study the temporal properties of the amplified mid-infrared pulses. Details of the EOS setup can be found in Supplementary Information section IV. Fig. 5(a) and (b) show the measured EOS traces and temporal intensities of the MIR pulses amplified in the OPA crystals with thicknesses giving the highest energies at the extrema of the MIR tunability range (see Fig. 4). The measured pulse durations are 148 fs at 4.7 μm and 73 fs at 8 μm. The 4.7 μm pulse can be compressed by removing the dispersion corresponding to 11 mm of Ge, yielding a duration of 122 fs, close to the FTL duration of 119 fs. The 8 μm pulse duration is 73 fs, close to the FTL duration of 69 fs. In terms of optical cycles, the measured pulse durations correspond to 9 and 2.5 optical cycles at the central wavelengths of 4.7 and 8 μm, respectively.

To conclude, we demonstrate an all inline two-stages MIR source based on iDFG and subsequent OPA, with pump recycling. It delivers 1 μJ, 73 fs (sub-three optical cycles) pulses at a 250 kHz repetition rate and a central wavelength of 8 μm, corresponding to a total energy efficiency of 2%, or a quantum efficiency of 15%. The amplified MIR is tunable over a large range from 4 to 8.5 μm. The presented technique has a very large applicability. A wide variety of iDFG and OPA crystals (LGS, $BaGa_4S_7$ [BGS], GaSe, $AgGaS_2$ [AGS], $ZnGeP_2$ [ZGP] as instances) can be used, regardless of the central wavelength of the pump pulse (for example around 800 nm, 1030 nm, or 2000 nm for Ti:Sa, ytterbium-based, holmium and thulium-based sources), as long as synchronization between the pulses involved in the nonlinear interaction is achieved with a birefringent crystal transparent for both signal and idler wavelengths. This architecture is compact and simple, combining high energy, broad bandwidth, and high repetition rate, particularly suitable for two-dimensional infrared spectroscopy experiments.

Funding. Agence Nationale de la Recherche (ANR) (ANR-10-LABX-0039-PALM, ANR-19-CE30-0001-MIRTHYX).

Disclosures. The authors declare no conflicts of interest.

Data Availability Statement. Data underlying the results presented in this Letter are not publicly available at this time but may be obtained from the authors upon reasonable request.

Supplemental document. See Supplement 1 for supporting content.

REFERENCES

1. S. Ghimire, A. D. DiChiara, E. Sistrunk, P. Agostini, L. F. DiMauro, and D. A. Reis, Nat. physics **7**, 138 (2011).
2. P. Dombi, Z. Pápa, J. Vogelsang, S. V. Yalunin, M. Sivis, G. Herink, S. Schäfer, P. Groß, C. Ropers, and C. Lienau, Rev. Mod. Phys. **92**, 025003 (2020).
3. I. Pupeza, M. Huber, M. Trubetskov, W. Schweinberger, S. A. Hussain, C. Hofer, K. Fritsch, M. Poetzlberger, L. Vamos, E. Fill, T. Amotchkina, V. K. Kepesidis, A. Apolonski, N. Karpowicz, V. Pervak, O. Pronin, F. Fleischmann, A. Azzeer, M. Žigman, and F. Krausz, Nature **577**, 52 (2020).
4. J. P. Ogilvie and K. J. Kubarych, Adv. In At. Mol. Opt. Phys. **57**, 249 (2009).
5. P. Hamm and M. Zanni, *Concepts and methods of 2D infrared spectroscopy* (Cambridge University Press, 2011).
6. M. K. Petti, J. P. Lomont, M. Maj, and M. T. Zanni, The J. Phys. Chem. B **122**, 1771 (2018).
7. B. M. Luther, K. M. Tracy, M. Gerrity, S. Brown, and A. T. Krummel, Opt. express **24**, 4117 (2016).
8. P. Donaldson, G. Greetham, D. Shaw, A. Parker, and M. Towrie, The J. Phys. Chem. A **122**, 780 (2018).
9. R. Fritzsch, P. M. Donaldson, G. M. Greetham, M. Towrie, A. W. Parker, M. J. Baker, and N. T. Hunt, Anal. chemistry **90**, 2732 (2018).
10. M. Seidel, X. Xiao, S. A. Hussain, G. Arisholm, A. Hartung, K. T. Zawilski, P. G. Schunemann, F. Habel, M. Trubetskov, V. Pervak, O. Pronin, and F. Krausz, Sci. advances **4**, eaaq1526 (2018).
11. S. B. Penwell, L. Whaley-Mayda, and A. Tokmakoff, Opt. letters **43**, 1363 (2018).
12. Z. Heiner, V. Petrov, and M. Mero, Opt. Lett. **45**, 5692 (2020).
13. R. Budriūnas, K. Jurkus, M. Vengris, and A. Varanavičius, Opt. Express **30**, 13009 (2022).
14. B.-H. Chen, E. Wittmann, Y. Morimoto, P. Baum, and E. Riedle, Opt. Express **27**, 21306 (2019).
15. S. Qu, H. Liang, K. Liu, X. Zou, W. Li, Q. J. Wang, and Y. Zhang, Opt. letters **44**, 2422 (2019).
16. Z. Heiner, V. Petrov, V. L. Panyutin, V. V. Badikov, K. Kato, K. Miyata, and M. Mero, Sci. Reports **12**, 1 (2022).
17. A. Bonvalet, M. Joffre, J. Martin, and A. Migus, Appl. Phys. Lett. **67**, 2907 (1995).
18. R. Kaindl, D. Smith, M. Joschko, M. Hasselbeck, M. Woerner, and T. Elsaesser, Opt. letters **23**, 861 (1998).
19. I. Pupeza, D. Sánchez, J. Zhang, N. Lilienfein, M. Seidel, N. Karpowicz, T. Paasch-Colberg, I. Znakovskaya, M. Pescher, W. Schweinberger, V. Pervak, E. Fill, O. Pronin, Z. Wei, F. Krausz, A. Apolonski, and J. Biegert, Nat. Photonics **9**, 721 (2015).
20. B.-H. Chen, T. Nagy, and P. Baum, Opt. Lett. **43**, 1742 (2018).
21. J. Liu, J. Ma, D. Lu, X. Gu, Z. Cui, P. Yuan, J. Wang, G. Xie, H. Yu, H. Zhang, and L. Qian, Opt. Lett. **45**, 5728 (2020).
22. A. Weigel, P. Jacob, D. Gröters, T. Buberl, M. Huber, M. Trubetskov, J. Heberle, and I. Pupeza, Opt. Express **29**, 20747 (2021).
23. Y. Yin, X. Ren, A. Chew, J. Li, Y. Wang, F. Zhuang, Y. Wu, and Z. Chang, Sci. reports **7**, 1 (2017).
24. N. Ishii, P. Xia, T. Kanai, and J. Itatani, Opt. express **27**, 11447 (2019).
25. M. Cronin-Golomb, Opt. letters **29**, 2046 (2004).
26. J. M. Fraser and C. Ventalon, Appl. optics **45**, 4109 (2006).
27. H. Fattahi, A. Schwarz, S. Keiber, and N. Karpowicz, Opt. letters **38**, 4216 (2013).
28. Q. Bournet, F. Guichard, M. Natile, Y. Zaouter, M. Joffre, A. Bonvalet, I. Pupeza, C. Hofer, F. Druon, M. Hanna, and P. Georges, Opt. Lett. **47**, 261 (2022).
29. L. Lavenu, M. Natile, F. Guichard, X. Délen, M. Hanna, Y. Zaouter, and P. Georges, Opt. express **27**, 1958 (2019).
30. M. Miranda, T. Fordell, C. Arnold, A. L'Huillier, and H. Crespo, Opt. express **20**, 688 (2012).

FULL REFERENCES

1. S. Ghimire, A. D. DiChiara, E. Sistrunk, P. Agostini, L. F. DiMauro, and D. A. Reis, "Observation of high-order harmonic generation in a bulk crystal," Nat. physics **7**, 138–141 (2011).
2. P. Dombi, Z. Pápa, J. Vogelsang, S. V. Yalunin, M. Sivis, G. Herink, S. Schäfer, P. Groß, C. Ropers, and C. Lienau, "Strong-field nano-optics," Rev. Mod. Phys. **92**, 025003 (2020).
3. I. Pupeza, M. Huber, M. Trubetskov, W. Schweinberger, S. A. Hussain, C. Hofer, K. Fritsch, M. Poetzlberger, L. Vamos, E. Fill, T. Amotchkina, V. K. Kepesidis, A. Apolonski, N. Karpowicz, V. Pervak, O. Pronin, F. Fleischmann, A. Azzeer, M. Żigman, and F. Krausz, "Field-resolved infrared spectroscopy of biological systems," Nature **577**, 52–59 (2020).
4. J. P. Ogilvie and K. J. Kubarych, "Multidimensional electronic and vibrational spectroscopy: An ultrafast probe of molecular relaxation and reaction dynamics," Adv. In At. Mol. Opt. Phys. **57**, 249–321 (2009).
5. P. Hamm and M. Zanni, *Concepts and methods of 2D infrared spectroscopy* (Cambridge University Press, 2011).
6. M. K. Petti, J. P. Lomont, M. Maj, and M. T. Zanni, "Two-dimensional spectroscopy is being used to address core scientific questions in biology and materials science," The J. Phys. Chem. B **122**, 1771–1780 (2018).
7. B. M. Luther, K. M. Tracy, M. Gerrity, S. Brown, and A. T. Krummel, "2d ir spectroscopy at 100 khz utilizing a mid-ir opcpa laser source," Opt. express **24**, 4117–4127 (2016).
8. P. Donaldson, G. Greetham, D. Shaw, A. Parker, and M. Towrie, "A 100 khz pulse shaping 2d-ir spectrometer based on dual yb: Kgw amplifiers," The J. Phys. Chem. A **122**, 780–787 (2018).
9. R. Fritzsch, P. M. Donaldson, G. M. Greetham, M. Towrie, A. W. Parker, M. J. Baker, and N. T. Hunt, "Rapid screening of dna–ligand complexes via 2d-ir spectroscopy and anova–pca," Anal. chemistry **90**, 2732–2740 (2018).
10. M. Seidel, X. Xiao, S. A. Hussain, G. Arisholm, A. Hartung, K. T. Zawilski, P. G. Schunemann, F. Habel, M. Trubetskov, V. Pervak, O. Pronin, and F. Krausz, "Multi-watt, multi-octave, mid-infrared femtosecond source," Sci. advances **4**, eaaq1526 (2018).
11. S. B. Penwell, L. Whaley-Mayda, and A. Tokmakoff, "Single-stage mhz mid-ir opa using ligas 2 and a fiber laser pump source," Opt. letters **43**, 1363–1366 (2018).
12. Z. Heiner, V. Petrov, and M. Mero, "Efficient, sub-4-cycle, 1-μm-pumped optical parametric amplifier at 10 μm based on baga 4 s 7," Opt. Lett. **45**, 5692–5695 (2020).
13. R. Budriūnas, K. Jurkus, M. Vengris, and A. Varanavičius, "Long seed, short pump: converting yb-doped laser radiation to multi-μj few-cycle pulses tunable through 2.5–15 μm," Opt. Express **30**, 13009–13023 (2022).
14. B.-H. Chen, E. Wittmann, Y. Morimoto, P. Baum, and E. Riedle, "Octave-spanning single-cycle middle-infrared generation through optical parametric amplification in ligas2," Opt. Express **27**, 21306–21318 (2019).
15. S. Qu, H. Liang, K. Liu, X. Zou, W. Li, Q. J. Wang, and Y. Zhang, "9 μm few-cycle optical parametric chirped-pulse amplifier based on ligas 2," Opt. letters **44**, 2422–2425 (2019).
16. Z. Heiner, V. Petrov, V. L. Panyutin, V. V. Badikov, K. Kato, K. Miyata, and M. Mero, "Efficient generation of few-cycle pulses beyond 10 μm from an optical parametric amplifier pumped by a 1-μm laser system," Sci. Reports **12**, 1–7 (2022).
17. A. Bonvalet, M. Joffre, J. Martin, and A. Migus, "Generation of ultrabroadband femtosecond pulses in the mid-infrared by optical rectification of 15 fs light pulses at 100 mhz repetition rate," Appl. Phys. Lett. **67**, 2907–2909 (1995).
18. R. Kaindl, D. Smith, M. Joschko, M. Hasselbeck, M. Woerner, and T. Elsaesser, "Femtosecond infrared pulses tunable from 9 to 18 μm at an 88-mhz repetition rate," Opt. letters **23**, 861–863 (1998).
19. I. Pupeza, D. Sánchez, J. Zhang, N. Lilienfein, M. Seidel, N. Karpowicz, T. Paasch-Colberg, I. Znakovskaya, M. Pescher, W. Schweinberger, V. Pervak, E. Fill, O. Pronin, Z. Wei, F. Krausz, A. Apolonski, and J. Biegert, "High-power sub-two-cycle mid-infrared pulses at 100 mhz repetition rate," Nat. Photonics **9**, 721–724 (2015).
20. B.-H. Chen, T. Nagy, and P. Baum, "Efficient middle-infrared generation in ligas 2 by simultaneous spectral broadening and difference-frequency generation," Opt. Lett. **43**, 1742–1745 (2018).
21. J. Liu, J. Ma, D. Lu, X. Gu, Z. Cui, P. Yuan, J. Wang, G. Xie, H. Yu, H. Zhang, and L. Qian, "Few-cycle pulses tunable from 3 to 7 μm via intrapulse difference-frequency generation in oxide lgn crystals," Opt. Lett. **45**, 5728–5731 (2020).
22. A. Weigel, P. Jacob, D. Gröters, T. Buberl, M. Huber, M. Trubetskov, J. Heberle, and I. Pupeza, "Ultra-rapid electro-optic sampling of octave-spanning mid-infrared waveforms," Opt. Express **29**, 20747–20764 (2021).
23. Y. Yin, X. Ren, A. Chew, J. Li, Y. Wang, F. Zhuang, Y. Wu, and Z. Chang, "Generation of octave-spanning mid-infrared pulses from cascaded second-order nonlinear processes in a single crystal," Sci. reports **7**, 1–7 (2017).
24. N. Ishii, P. Xia, T. Kanai, and J. Itatani, "Optical parametric amplification of carrier-envelope phase-stabilized mid-infrared pulses generated by intra-pulse difference frequency generation," Opt. express **27**, 11447–11454 (2019).
25. M. Cronin-Golomb, "Cascaded nonlinear difference-frequency generation of enhanced terahertz wave production," Opt. letters **29**, 2046–2048 (2004).
26. J. M. Fraser and C. Ventalon, "Parametric cascade downconverter for intense ultrafast mid-infrared generation beyond the manley-rowe limit," Appl. optics **45**, 4109–4113 (2006).
27. H. Fattahi, A. Schwarz, S. Keiber, and N. Karpowicz, "Efficient, octave-spanning difference-frequency generation using few-cycle pulses in simple collinear geometry," Opt. letters **38**, 4216–4219 (2013).
28. Q. Bournet, F. Guichard, M. Natile, Y. Zaouter, M. Joffre, A. Bonvalet, I. Pupeza, C. Hofer, F. Druon, M. Hanna, and P. Georges, "Enhanced intrapulse difference frequency generation in the mid-infrared by a spectrally dependent polarization state," Opt. Lett. **47**, 261–264 (2022).
29. L. Lavenu, M. Natile, F. Guichard, X. Délen, M. Hanna, Y. Zaouter, and P. Georges, "High-power two-cycle ultrafast source based on hybrid nonlinear compression," Opt. express **27**, 1958–1967 (2019).
30. M. Miranda, T. Fordell, C. Arnold, A. L'Huillier, and H. Crespo, "Simultaneous compression and characterization of ultrashort laser pulses using chirped mirrors and glass wedges," Opt. express **20**, 688–697 (2012).